Ultrafast magnetization and energy flow in the laser-induced dynamics of transition metal compounds

G. Stegmann, W. Töws, and G. M. Pastor
Institut für Theoretische Physik, Universität Kassel, 34132 Kassel, Germany

(Received 15 September 2021; revised 2 December 2022; accepted 1 February 2023; published 10 February 2023)

An electronic theory of the laser-induced ultrafast magnetization dynamics in transition-metal alloys is presented. A many-body model Hamiltonian is considered that incorporates the fundamental electronic hopping, local Coulomb interaction, and spin-orbit coupling (SOC) on the same footing. Exact time propagations are performed on a tetrahedral cluster, from which the time dependencies of the local spin moments, orbital occupations, and single-particle energies of homogeneous systems and binary alloys are obtained. The consequences of inhomogeneities in the laser absorption and in the SOC strengths are investigated giving emphasis to the nature of spin-density transfers between the alloy components. A local perspective on the optically induced spin transfer is proposed in terms of which two main steps emerge: a dominantly local optical excitation followed by hopping-driven spin-density transfers among the different alloy components. The conjoint action of the spin-orbit interactions at the origin of local spin flips and spin-to-orbital angular-momentum transfer and the interatomic hoppings responsible for charge, spin, and energy flows between different sublattices is demonstrated. Transient and steady-state dynamical regimes are identified that result in delays in the onset of the local demagnetizations and in ultrafast redistributions of the spin. The central role of electron delocalization and electronic hopping in the spin-density redistribution and demagnetization of the different alloy components is demonstrated.

DOI: 10.1103/PhysRevB.107.054410

I. INTRODUCTION

More than two decades ago, Beaurepaire *et al.* observed the laser-induced ultrafast demagnetization (UFD) of a ferromagnetic (FM) transition-metal (TM) in the case of Ni films [1]. This remarkable experiment started an extremely intense experimental and theoretical research activity in the field of magneto-optics, which has provided unique insights into the fundamental quantum mechanical processes controlling the magnetization dynamics on a subpicosecond timescale. In past years numerous time- and element-resolved measurements of the dynamical response to ultrashort laser pulses have been performed on transition-metal and rare-earth (RE) compounds including alloys and multilayers. In these studies not only the fundamental aspects of the laser-induced magnetization dynamics have been investigated, but also several potential applications of ultrafast magnetization control in spin-electronic devices have been identified. Understanding the many-body dynamics underlying the UFD effect is central to achieving a controlled ultrafast manipulation of the magnetization. Consequently, important theoretical research effort has been devoted to explaining this phenomenon. In this context a number of different, partly complementary physical mechanisms have been proposed, including magneto-optical absorption [2,3], electron-electron scattering [4,5], electron-magnon interaction [6–9], electron-phonon spin-flip scattering [10–20], superdiffusive spin-polarized electron transport [21–25], intersite spin exchange [26–28], and electronic processes driven by the spin-orbit coupling (SOC) [29–37].

Recently, researchers' attention has been increasingly focused on magnetic alloys and multilayers, where the interplay between different elements and different local environments comes into play. Time-resolved element-specific experiments have been performed by using x-ray magnetic circular dichroism (XMCD) techniques [38–48] or the transversal magneto-optical Kerr effect [23,48–63]. In this way a number of novel alloy-specific phenomena have been revealed that are not present in homogeneous ferromagnets, for example, the all-optical magnetization switching observed in the ferrimagnetic GdFeCo and MnRuGa alloys [39,40,51,63–66], the laser-induced interlayer spin transfer [67], and the optically induced spin transfer (OISTR) [31,68], which has been theoretically and experimentally observed in a variety of compounds [31,37,44–46,62,68–70].

Quite generally, the inhomogeneities which are inherent to alloys on the atomic scale result in very interesting element-specific time evolutions of the magnetization density. For instance, element-specific demagnetization times have been observed in GdFeCo, FeNi, CoPt, and FePt alloys [39,41,55,56]. Furthermore, Mathias *et al.* observed a delay in the demagnetization response of Ni in $Ni_{80}Fe_{20}$ (permalloy), i.e., a time shift with respect to the Fe demagnetization [50]. Further measurements in permalloys by Günther *et al.*, Jana *et al.,* and Möller *et al.* confirmed the presence of a delay in the demagnetization of Ni with respect to Fe [48,57–59]. An analogous behavior has also been observed in FeRh alloys. In this case the Fe demagnetization is delayed with respect to that of Rh [57]. However, notice that no delay in the onset of the demagnetization of Ni has been observed in

the experiments by Radu *et al.* [41] and by Liu *et al.* [60], although Ni is found to demagnetize slower in the permalloy than in pure Ni. Further insights on alloy-specific behaviors have been obtained in the works by Graves *et al.* and Bergeard *et al.* on TM-RE compounds such as GdFeCo, CoGd, and CoTb [42,51]. In this case one observes that a dissipationless redistribution of spin density between sublattices contributes significantly to the magnetization dynamics, particularly during the first few hundreds of femtoseconds after the laser excitation.

These remarkable dependencies on the composition, stoichiometry, and structure demonstrate the importance of the juxtaposition of alloy components with contrasting characteristics and of the resulting interplay between different local atomic environments. Understanding the microscopic mechanisms of the magnetization dynamics in alloys and multilayers is particularly challenging, since it involves both local demagnetization processes as well as exchanges of electrons, energy, and angular momentum between the different material components.

A number of theoretical works have addressed the magnetization dynamics of inhomogeneous magnetic materials and the microscopic mechanisms behind them. Several authors have explained the UFD in multicomponent systems as the result of intersite spin exchange and heat-induced local demagnetization, which are described either in terms of rate equations or by performing Landau-Lifshitz-Gilbert simulations [26–28,39–41]. Schellekens and Koopmans have proposed a microscopic model of multicomponent magnetic materials by considering electron-phonon spin-flip scattering as the driving mechanism of the local demagnetization process [16]. Thus, the ultrafast magnetization switching in ferrimagnetic TM-RE alloys [39,64] and the delay of the Ni demagnetization in permalloys [50] have been explained by taking into account element-specific electron-phonon spin-flip rates. More recently, Dewhurst *et al.* have performed time-dependent density-functional calculations, showing that the OISTR effect can lead to an ultrafast switching of the magnetic order in several TM compounds [68]. In this work the authors have demonstrated how a direct spin-conserving interatomic excitation can lead to an important ultrafast redistribution of the spin-polarized density between the different sublattices during the duration of the laser pulse, which dominates the early stages of the spin dynamics. These remarkable findings motivate further theoretical investigations of the OISTR effect from a local perspective. In particular it would be interesting to understand how any element specificities concerning, for example, the optical absorptions, the spin-to-orbital angular-momentum transfers and the intersite spin transfers affect the alloy-magnetization dynamics as a whole. Moreover, in the case of TM compounds, one would like to elucidate how the energy and spin-density redistributions taking place during and shortly after the laser pulse are mediated by the itinerant electrons responsible of magnetism.

The purpose of this paper is to investigate the laser-induced magnetization dynamics of binary TM alloys from a local many-body perspective by extending a previously proposed electronic theory [30] to multicomponent systems. In Sec. II the considered *pd*-band model Hamiltonian is described that takes into account the interplay between hybridizations, Coulomb interactions, and spin-orbit couplings. Details on the calculations of the magnetic response to optical excitations as a function of the microscopic model parameters are given in Sec. III. The results of exact time propagations are presented and discussed in Sec. IV. The role of inhomogeneities in the laser absorptions and in the SOC strengths, as well as the importance of hybridizations and spin-carrying electronic motion, are quantified. In particular it is shown how the demagnetization times and any possible demagnetization delays depend on the element-specific spin-orbit coupling strengths, on the local environment of the atoms, and on the spin-density transfer between the sublattices. In this way, a strong interdependence between the local magnetization dynamics of the different alloy components is revealed.

II. MANY-BODY MODEL OF TRANSITION METAL ALLOYS

In order to investigate the laser-induced electronic dynamics in TM alloys we consider the *pd*-model Hamiltonian

$$\hat{H} = \hat{H}_0 + \hat{H}_C + \hat{H}_{\mathrm{SO}} + \hat{H}_E(t), \tag{1}$$

which extends the one proposed in Ref. [30]. The first term,

$$\hat{H}_0 = \sum_{i\alpha\sigma} \varepsilon_{i\alpha} \hat{c}^\dagger_{i\alpha\sigma} \hat{c}_{i\alpha\sigma} + \sum_{ij\alpha\beta\sigma} t^{\alpha\beta}_{ij} \hat{c}^\dagger_{i\alpha\sigma} \hat{c}_{j\beta\sigma}, \tag{2}$$

describes the single-particle hybridizations of the valence electrons yielding electron delocalization and metallic behavior. The operator $\hat{c}^\dagger_{i\alpha\sigma}(\hat{c}_{i\alpha\sigma})$ creates (annihilates) an electron with spin σ at the orbital α of atom i, where $\alpha \equiv nlm$ corresponds to well-defined radial, orbital, and magnetic quantum numbers. The model takes into account the $3d$ electrons, which are responsible for the magnetic behavior and the $4p$ electrons, which are directly involved in optical excitations of the $3d$ band. The second term,

$$\hat{H}_C = \frac{1}{2}\sum_i U_i\, \hat{n}^d_i \left(\hat{n}^d_i - 1\right) - \sum_i J_i\, \hat{\boldsymbol{s}}^d_i \cdot \hat{\boldsymbol{s}}^d_i, \tag{3}$$

takes into account the dominant intra-atomic Coulomb interactions among the d electrons, where $\hat{n}^d_i$ and $\hat{\boldsymbol{s}}^d_i$ are, respectively, the total d-electron number operator and spin operator at atom i. Accordingly U_i and J_i denote the average direct and exchange d-electron Coulomb integral at atom i. The third term,

$$\hat{H}_{\mathrm{SO}} = \sum_i \xi_i \sum_{\alpha\beta\sigma\sigma'} (\boldsymbol{l}\cdot\boldsymbol{s})_{\alpha\sigma,\beta\sigma'}\, \hat{c}^\dagger_{i\alpha\sigma}\, \hat{c}_{i\beta\sigma'}, \tag{4}$$

describes the SOC of the d electrons, where $(\boldsymbol{l}\cdot\boldsymbol{s})_{\alpha\sigma,\beta\sigma'}$ stands for the intra-atomic matrix elements of $\boldsymbol{l}\cdot\boldsymbol{s}$ and ξ_i defines the SOC strength at atom i. Notice that the sum over α and β in Eq. (4) involves only the d orbitals. Finally, the last term in Eq. (1) is given by

$$\hat{H}_E(t) = e\mathbf{E}(t)\cdot \sum_{i\alpha\beta\sigma} \langle i\alpha|\hat{\mathbf{r}}|i\beta\rangle \hat{c}^\dagger_{i\alpha\sigma}\, \hat{c}_{i\beta\sigma}, \tag{5}$$

which represents the interaction with the external laser field $\mathbf{E}(t)$ in the intra-atomic dipole approximation. The usual

atomic selection rules for the position operator $\hat{\mathbf{r}}$ imply that only pd and dp transitions enter the sum.

Before closing this section, it is important to remark that no *ad hoc* phenomenological spin relaxation terms or mean-field approximations are involved in the model, which would break the spin-rotational invariance of $\hat{H}$. In fact, the Hamiltonian given by Eqs. (1)–(5) satisfies all the fundamental electronic conservation laws [30]. The single-particle term $\hat{H}_0$, the Coulomb interaction $\hat{H}_C$, and the dipole interaction with the laser field $\hat{H}_E$ conserve the total spin $\boldsymbol{S} = \sum_i \boldsymbol{s}_i$ ($[\hat{H}_0, \hat{\mathbf{S}}] = [\hat{H}_C, \hat{\mathbf{S}}] = [\hat{H}_E, \hat{\mathbf{S}}] = 0$). Only the SOC breaks the spin conservation ($[\hat{H}_{\mathrm{SO}}, \hat{\mathbf{S}}] \neq 0$) while preserving the total local angular momentum $\hat{\boldsymbol{l}}_i + \hat{\boldsymbol{s}}_i$ at each atom i ($[\hat{H}_{\mathrm{SO}}, \hat{\boldsymbol{l}}_i + \hat{\boldsymbol{s}}_i] = 0$). Notice, moreover, that $\hat{H}_0$ preserves neither the local $\hat{\boldsymbol{l}}_i$ nor the total orbital moment $\hat{\boldsymbol{L}} = \sum_i \hat{\boldsymbol{l}}_i$, since the interatomic hoppings describe the interaction of the electrons with the lattice potential, which is not rotational invariant ($[\hat{H}_0, \hat{\boldsymbol{l}}_i] \neq 0$ and $[\hat{H}_0, \hat{\boldsymbol{L}}] \neq 0$). These fundamental commutation rules (conservation and nonconservation laws) are very useful in order to understand qualitatively the roles played by the SOC, Coulomb interaction, and electron delocalization in the dynamics of magnetic alloys.

III. COMPUTATIONAL DETAILS

For the applications we consider a tetrahedral cluster model, for which the exact solution of the ground state and subsequent time evolutions can be numerically obtained. The cluster is divided in the sublattices A and B, as illustrated in the inset of Fig. 1, which corresponds to a 50% concentration in a binary alloy such as FeNi. As in Ref. [30], the degeneracy of the bands is reduced in order to limit the numerical effort by considering only three $3d$ orbitals per atom ($m = -1$, 0, and 1) and one $4p$ orbital per atom ($m = 0$). The nearest-neighbor (NN) hopping integrals are taken from band-structure calculations [71]. For simplicity, the direct Coulomb integrals $U_i = 10$ eV, exchange integrals $J_i = 2$ eV, and dp promotion energy $\Delta\varepsilon_{pd} = 1$ eV are assumed to be the same for both elements. The spin-orbit-coupling strength ξ_i is varied systematically around the reference value $\xi = 50$ meV corresponding to homogeneous transition metals [72]. These parameters yield a FM ground state of the alloy with an almost saturated spin polarization per atom $S_z \simeq 0.61\ \hbar$ and a small $4p$-band occupation $n_p \simeq 0.03$. The exact time evolutions of the many-electron wave function are calculated numerically by means of short-time iterative Lanczos propagations [73]. The dependence of the electronic dynamics on the microscopic interaction parameters characterizing the different alloy components is quantified by contrasting homogeneous and inhomogeneous optical absorptions and by varying the strength of the local spin-orbit couplings and of the interatomic hybridizations.

The initial excitation is triggered by the time-dependent electric laser field $\mathbf{E}$ [see Eqs. (1) and (5)] which we assume to have a Gaussian envelope with a standard deviation $\tau_p = 1$ fs. Choosing such a short pumping pulse has the advantage that the excitation is almost completely over, before any significant intrinsic magnetization dynamics takes place. In this way the initial absorption is clearly separated from the subsequent relaxation. In addition, calculations have been performed for longer pulses up to $\tau_p = 80$ fs. These show, in agreement with Ref. [34], that the precise value of τ_p does not affect qualitatively the time dependence of the sublattice magnetizations after the laser pulse. Short pumping pulses have also the practical advantage of distributing the absorbed energy over a relatively broad energy range ΔE (in the present case $\Delta E \simeq 0.6$ eV since $\Delta t \simeq \tau_p = 1$ fs) which renders the absorption less sensitive to the details of the energy spectrum of the cluster model used for the numerical propagations. The considered laser wave length of $\lambda = 1050$ nm is in the experimentally relevant range where the absorption is significant. The fluence is such that the absorbed energy amounts to 225 meV/atom. It has been verified that the precise value of λ does not alter the postexcitation dynamics in any significant way [34].

In order to analyze the microscopic processes involved in the magnetization dynamics of the alloys and to identify any element specific behaviors, it is very useful to vary the different model parameters independently and to compare the corresponding magnetic responses. However, any changes in the interaction parameters also imply some changes in the electronic structure of the alloy and its optical absorption, which are likely to mask or distort, at least to some extent, the actual role of the microscopic process under study [74]. Therefore, in Secs. IV B and IV E, we compare the dynamics of alloys with different microscopic parameters by starting from the same initial electronic state. An appropriate unbiased choice is the laser excited state of a homogeneous reference system at time $t = 1$ fs. The subsequent time propagations ($t \geqslant 1$ fs) are derived according to the field-free Hamiltonian of the corresponding alloy. In this way the focus is set on the element-specific spin dynamics and on the roles played by the different electronic interactions, which are the main goals of the present work.

IV. RESULTS AND DISCUSSION

In this section we take advantage of the flexibility of our model Hamiltonian in order to investigate (i) the consequences of an inhomogeneous laser absorption, which conditions the initial excited state; (ii) the role of element-specific SOC strengths, which controls the spin-to-orbital angular-momentum transfer rate; (iii) the nature of the spin-density flow between the sublattices during the demagnetization process; and (iv) the importance of the environment-dependent interatomic hoppings, which are at the origin of the spin-density transfer between the different alloy components.

A. Inhomogeneous laser-pulse absorption

We consider an idealized extremely inhomogeneous excitation, in which all the laser absorption takes place on the atoms of sublattice A. This is achieved by setting the optical-transition matrix elements $\langle i\alpha|\hat{\mathbf{r}}|i\beta\rangle = 0$ for the atoms of sublattice B, while keeping $\langle i\alpha|\hat{\mathbf{r}}|i\beta\rangle$ in the sublattice A as in the homogeneous case. The resulting spin dynamics is compared with the corresponding homogeneous excitation, in which $\langle i\alpha|\hat{\mathbf{r}}|i\beta\rangle$ is the same on all atoms. Since the total absorbed energy has a strong influence on the degree of demagnetization at long times [34] we reduce the laser fluence

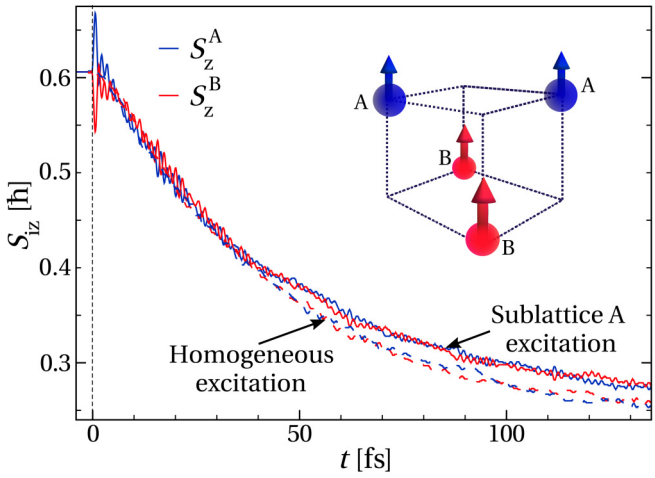

FIG. 1. Time dependence of the average spin magnetization $S_{iz}(t)$ of sublattice A (blue curves) and sublattice B (red curves) after an inhomogeneous laser pulse acting only on sublattice A (solid curves) and after a homogeneous absorption in both sublattices (dashed curves). The pulse is centered at $t = 0$ and has a duration $\tau_p = 1$ fs. The inset shows the tetrahedral cluster used for the exact time propagations.

by $\simeq$27% in the homogeneous case in order that the total absorbed energy $\Delta\mathcal{E} \simeq 225$ meV/atom is the same in both cases. All other laser and material parameters, in particular $\xi = 50$ meV, are assumed to be the same for both elements, as given in Sec. III.

Figure 1 shows the time dependence of the average spin projections $S_{iz}(t) = \langle \hat{S}_{iz} \rangle$ at the two sublattices. Starting from the nearly saturated ground state a remarkable ultrafast magnetization dynamics unfolds, which is qualitatively similar to previous calculations on homogeneous systems [30,34]. This applies in particular to the degree of demagnetization, from $S_{iz} \simeq 0.6\ \hbar$ to $S_{iz} \simeq 0.3\ \hbar$, and to the demagnetization time which is of the order of 50–100 fs. Qualitatively, the UFD of the alloys can be explained to be the result of three main local and semilocal contributions, which are analogous to the homogeneous case considered in Ref. [30]. First, the initial excitation creates *pd* electron-hole pairs, which open new channels for electronic transitions between majority-spin and minority-spin states of comparable energy. Following the optically induced occupation changes, an angular-momentum transfer from the spin to the orbital electronic degrees of freedom sets in. This process is driven by the spin-orbit interactions and therefore involves a characteristic timescale of the order of $\tau_{\rm SOC} \simeq \hbar/\xi \simeq 13$ fs. At the same time, any incipient increase of the local orbital angular momenta $\boldsymbol{l}_i$, due to the decrease of $\boldsymbol{s}_i$, is very rapidly, though not instantaneously counteracted by the delocalization of the electrons throughout the lattice [30]. This orbital-moment quenching takes place at the much shorter timescale $\tau_{\rm hop} \simeq \hbar/t_{ij} \simeq 0.6$ fs, which is controlled by the hopping integrals t_{ij} responsible for the interatomic hybridizations ($t_{ij} \simeq 1$ eV). The net result is the decrease of the spin magnetization at a rate roughly proportional to $\hbar/\xi$, without any lasting increase of the local orbital moments on the timescale of the demagnetization $\tau_{\rm dm} \simeq 50$–100 fs [43]. In this context it is interesting to note that the above model explanation of the UFD effect is consistent with recent DFT calculations of the time dependence of the orbital magnetic moments of Ni and Co films at the early stages of the dynamics [36]. Both model and first principles theoretical results are in agreement with the spin-orbit origin of the ultrafast demagnetization and the experimental observation, using XMCD, that the electronic orbital degrees of freedom are no reservoir of angular momentum owing to orbital-moment quenching [30,43,75–77].

Despite the general validity of the above-mentioned arguments, it is still quite remarkable that the time dependencies of S_z^A and S_z^B are so similar, even if the optical absorption occurs only on sublattice A. Indeed, except at the very early stages of the dynamics to be discussed below (i.e., for $0 < t \lesssim 5$ fs) any inhomogeneity in the initial excited many-body state is rapidly washed away within only a few femtoseconds, having no significant influence on the rate of change of S_{iz} on the timescale of the UFD effect ($\tau_{\rm dm} = 50$–100 fs). Moreover, the time dependence of S_{iz} following the inhomogeneous laser absorption on sublattice A is nearly the same as in the case of a perfectly homogeneous absorption, excluding again the very short initial times (compare solid and dashed curves in Fig. 1). We conclude that differences in the optical absorptions of the material components have no significant influence on the ultrafast laser-induced demagnetization of itinerant-electron FM alloys.

In order to identify similarities and differences between the time dependencies of S_z^A and S_z^B, it is useful to analyze the spin dynamics during the optical absorption and the following few femtoseconds. In Fig. 2 we focus on these early stages of the dynamics, where significant differences in the local spin polarizations and in other local properties are revealed. For the inhomogeneous excitation one observes that the spin magnetization of the directly excited sublattice A *increases* from $S_z^A = 0.606\ \hbar$ to $0.668\ \hbar$ as soon as the pulse goes over its maximum intensity [compare the solid blue curve with the pulse shape in Fig. 2(a)]. At the same time the spin magnetization of sublattice B, which is not directly excited by the pulse, *decreases* by the same amount from $S_z^B = 0.606\ \hbar$ to $S_z^B = 0.543\ \hbar$ (solid red curve). This reveals an extremely rapid majority spin-density flow from the sublattice B, where the local orbital occupations are not directly affected by the laser pulse, toward sublattice A, where holes in the majority spin band are created by the d to p optical absorption. Once this spin imbalance is triggered, some oscillations of both S_z^A and S_z^B follow on a femtosecond timescale, which are then progressively damped. Further complementary information is provided by the corresponding local numbers of electrons n_{iT} and by the local numbers of majority-spin d electrons $n_{id\uparrow}$ shown in Fig. 2(b). In all these cases the sublattices A and B show opposite out-of-phase trends, the one increasing while the other decreases and vice versa.

This remarkable short-time dynamics can be rationalized as follows. At the very beginning of the excitation, the laser pulse induces mainly intra-atomic transitions of the majority (up) d electrons of sublattice A into the nearly empty p orbitals. Subsequently, about 0.5 fs later, the up d holes left behind on sublattice A are partly filled as a result of electronic hopping from sublattice B. These two processes manifest themself as a decrease of $n_{d\uparrow}^A$, which matches the

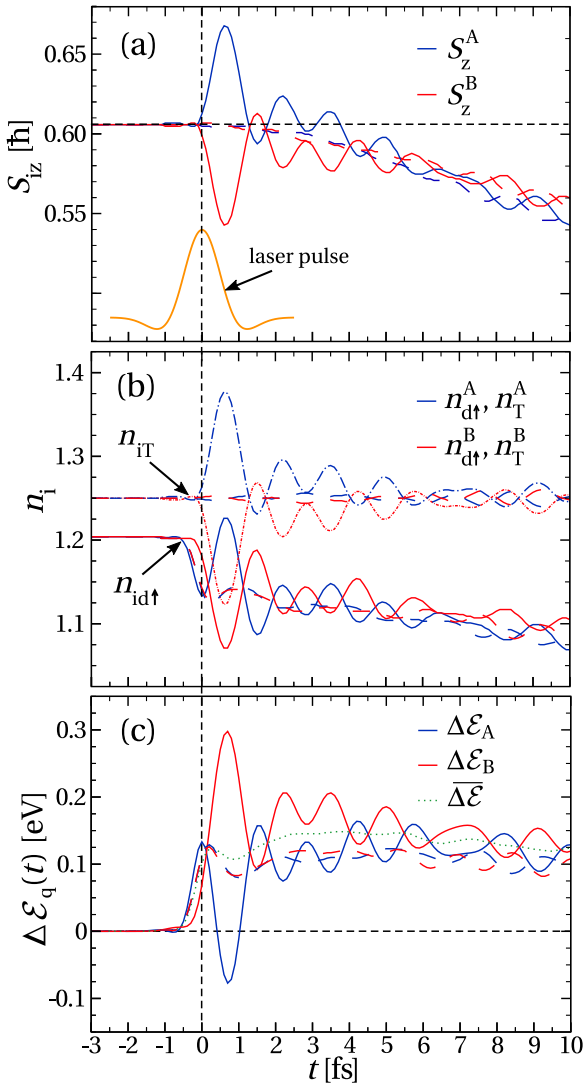

FIG. 2. Time dependence of (a) the local spin polarization S_{iz}, (b) the majority-spin d-electron (total electron) occupations $n_{id\uparrow}$ (n_{iT}), and (c) the local absorbed excitation energies $\Delta\mathcal{E}_q(t) = \mathcal{E}_q(t) - \mathcal{E}_q^0$ corresponding to the sublattices A (blue curves) and B (red curves). Results are given for an inhomogeneous laser absorption on sublattice A (solid curves) and a homogeneous laser absorption on both sublattices (dashed curves). The dotted curve in (c) shows the average absorbed energy $\overline{\Delta\mathcal{E}} = (\Delta\mathcal{E}_A + \Delta\mathcal{E}_B)/2$ in the inhomogeneous case. The pulse is centered at $t = 0$ and has a duration of $\tau_p = 1$ fs as illustrated in (a).

shape of the laser pulse, followed by an increase of n_T^A for $t > 0$. Notice that the increase in n_T^A is delayed with respect to the absorption-induced decrease of $n_{d\uparrow}^A$, since it can only take place after a significant number of holes are created in the d band of sublattice A. This initial magnetization and charge imbalance between the two sublattices triggers rapid, eventually damped oscillations of S_{iz}, n_{iT}, and $n_{id\uparrow}$, which are the consequence of electron delocalization. It is important to stress that the total spin $S_z^A + S_z^B$ remains almost perfectly conserved during all these early dynamical processes. Indeed, the total spin conservation is granted both by the optical absorptions and by the electronic hoppings responsible for the interatomic spin and charge flow. Furthermore, note that on the timescale of only a few femtoseconds, the effect of the SOC on the local spin polarizations, even if present, is not quantitatively important ($\hbar/\xi \simeq 13$ fs). Therefore, no significant demagnetization can follow and $S_z^A + S_z^B$ is nearly perfectly conserved.

The above discussed hopping-driven spin-density flow deserves to be compared with the OISTR reported in Refs. [31,62,68] in order to emphasize analogies and differences. The OISTR effect has been first predicted in TD-DFT alloy and multilayer studies [31,68] and has also been experimentally observed in FeNi alloys [62]. In the case of FeNi and according to Ref. [62], it is the result of all-optical and thus ultrafast transitions from occupied minority-spin delocalized Bloch states, whose weight in the local density of electronic states (DOS) lies predominantly on the Ni sublattice, to unoccupied delocalized states having the same spin but whose spectral weight lies mainly on the Fe sublattice. In our model the optical absorption is strictly intra-atomic [see Eq. (5)]. Therefore, setting the parameter $\langle i\alpha|\hat{\mathbf{r}}|i\beta\rangle = 0$ at sublattice B implies that the laser excitation can only change the orbital occupations at the A atoms. Consequently, the OISTR appears in our calculations as a two step process: The creation of majority-spin d holes on sublattice A followed by a very fast spin-conserving hopping from sublattice B. The process is indeed very fast, as fast as the typical optical excitation itself since the characteristic hopping times in TMs are very small ($\tau_{\text{hop}} \simeq \hbar/t_{ij} \simeq 1$ fs). Our model calculations thus provide a real-space local perspective to the OISTR effect, which is complementary to the original band structure or Kohn-Sham picture [31,68]. From the delocalized perspective, the spin-density transfer appears as a purely optical process, although the electronic hoppings and interatomic hybridizations underly the corresponding band structure and local DOS. Despite the differences which are inherent to the real-space versus k-space duality, we believe that both local and band descriptions of the OISTR reflect the same microscopic quantum processes, namely spin-conserving optical absorption and interatomic hybridizations.

In addition to the fluctuation and reequilibration of the local spin magnetizations S_{iz} and electronic densities n_{iT}, one would like to understand how the inhomogeneously absorbed energy is redistributed within the alloy. To this aim we calculated the sublattice excitation energies $\Delta\mathcal{E}_q(t) = \mathcal{E}_q(t) - \mathcal{E}_q^0$, where the sublattice energy $\mathcal{E}_q(t)$ and its corresponding ground-state value $\mathcal{E}_q^0$ are obtained by averaging the field-free Hamiltonian of each sublattice excluding the hybridizations between the sublattices:

$$\mathcal{E}_q(t) = \frac{1}{N_q}\langle\psi(t)|\,\hat{H}_0^q + \hat{H}_C^q + \hat{H}_{\text{SO}}^q\,|\psi(t)\rangle,$$

where $\hat{H}_0^q$, $\hat{H}_C^q$, and $\hat{H}_{\text{SO}}^q$ are given by Eqs. (2)–(4) including only the orbitals which belong to sublattice q and N_q is the number of sublattice atoms. Notice that $|\psi(t)\rangle$ stands for the many-body Schrödinger ket, whose time dependence follows the complete Hamiltonian $\hat{H}$ given by Eqs. (1)–(5).

In Fig. 2(c) the sublattice excitation energies $\Delta\mathcal{E}_A$ and $\Delta\mathcal{E}_B$ are shown as a function of time. The solid (dashed) curves correspond to an inhomogeneous (homogeneous) excitation and the dotted curve indicates the alloy average

$\overline{\Delta\mathcal{E}} = (\Delta\mathcal{E}_A + \Delta\mathcal{E}_B)/2$ in the inhomogeneous case. One observes that the time dependence of $\Delta\mathcal{E}_A(t)$ [$\Delta\mathcal{E}_B(t)$] correlates very well with the corresponding time dependence of the d-electron occupation number $n^A_{d\uparrow}$ [$n^B_{d\uparrow}$]. During the laser pulse $\Delta\mathcal{E}_A$ increases until the Gaussian-shaped pulse and the $d\uparrow$ to p promotion within sublattice A reach their peak [compare Figs. 2(b) and 2(c)]. The subsequent decrease of $\Delta\mathcal{E}_A$ until the end of the laser pulse is a consequence of the strong spin-up electron transfer from sublattice B, as described above. The filling of the up d holes in sublattice A leads to a significant decrease of $\Delta\mathcal{E}_A$ and at the same time to an increase of $\Delta\mathcal{E}_B$. These time-dependent trends reflect the dominant role that the d electrons play in the alloy binding.

The oscillations of $\Delta\mathcal{E}_A(t)$ and $\Delta\mathcal{E}_B(t)$ are strongly damped only a few femtoseconds after the laser excitation, as the absorbed energy is evenly redistributed throughout the alloy. Once the sublattice energies become nearly the same, the system has lost almost all memory of the strong inhomogeneity of the initial energy absorption. These rapid local-energy and spin-density reequilibrations, which take place on a timescale of the order of $\tau_{\text{hop}} \simeq 1$ fs, explain why the subsequent demagnetization process is quite insensitive to any inhomogeneity in the laser excitation (see Fig. 1). Any possible initial absorption differences between the alloy components are not very relevant for the subsequent magnetization dynamics, since they are very rapidly washed out by the itinerant nature of the electronic states and by the Coulomb interactions among the electrons.

Although achieving femtosecond time resolution is a serious current experimental challenge, it is important to theoretically investigate the limit of very short pumping pulses in order to reveal the dynamics of the redistribution of the optically absorbed energy between the sublattices A and B, which are much more difficult to see when the pulse duration is longer than the hopping timescale τ_{hop}. Indeed, the large-amplitude, short-time oscillations of the electron density between NN atoms belonging to the laser-absorbing and nonabsorbing alloy components are observed only when the pumping pulse is very short. In Fig. 2, the pulse duration $\tau_p = 1$ fs is comparable to the typical NN electron hopping time $\tau_{\text{hop}} \simeq 0.6$ fs for hopping integrals of the order of 1 eV. Calculations for longer pulse durations $\tau_p \geqslant 20$ fs do not show such strong short-time effects, even for the most heterogeneous absorption. For example, in Fig. 3 results are given for the time dependence of the sublattice occupation numbers and local absorbed energies obtained for a pulse duration $\tau_p = 20$. In this case one observes that the differences in the local occupations $n_{id\uparrow}$ and n_{iT}, as well as in the local absorbed excitation energy $\Delta\mathcal{E}_q$, following the inhomogeneous laser absorption are much less important. In particular the short-time quantum oscillations due to the electronic hopping have a much smaller amplitude, which does not affect the general trend.

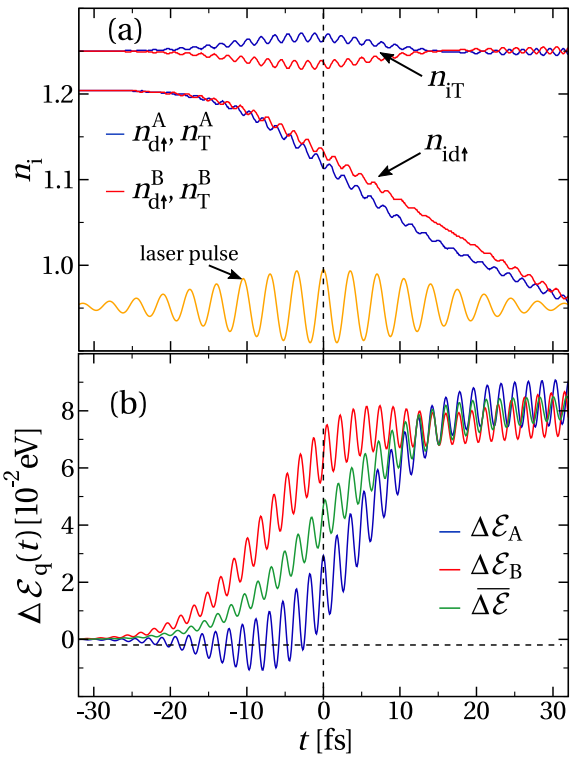

FIG. 3. Time dependence of (a) the majority-spin d-electron (total electron) occupations $n_{id\uparrow}$ (n_{iT}) and (b) the local absorbed excitation energies $\Delta\mathcal{E}_q(t) = \mathcal{E}_q(t) - \mathcal{E}^0_q$ corresponding to the sublattices A (blue curves) and B (red curves). Results are given for an inhomogeneous laser absorption on sublattice A. The green curve in (b) shows the average absorbed energy $\overline{\Delta\mathcal{E}} = (\Delta\mathcal{E}_A + \Delta\mathcal{E}_B)/2$. The pulse is centered at $t = 0$ and has a duration of $\tau_p = 20$ fs as illustrated in (a).

B. Inhomogeneous SOC strength

The spin-orbit interaction defines the fundamental channel for the angular momentum transfer between spin and orbital electronic degrees of freedom and therefore plays a central role in the UFD effect [30]. Consequently, it is most interesting to investigate the laser-induced magnetization dynamics in alloys which combine elements with different SOC strengths. For this purpose we consider in the following element-specific ξ_i keeping all other material and laser-absorption parameters the same for both elements, as given in Sec. III. The SOC strength ξ_A of sublattice A is systematically varied in the range $0 \leqslant \xi_A \leqslant 210$ meV, while in sublattice B $\xi_B = 50$ meV is kept constant (see also the inset of Fig. 1) [78] In magnetic TMs like Fe, Co, and Ni the SOC constants ξ are very similar [72]. Nevertheless, the efficiencies of local spin-orbit transitions can differ strongly, since they depend on the details of the DOS and occupation numbers after excitation. For simplicity, these differences in SOC efficiency are modeled in this work by varying ξ_A and ξ_B. In order to isolate and identify the consequences of varying ξ_A on the electronic dynamics we consider the same initial excited state in all cases, which corresponds to the laser excitation of the homogeneous system having $\xi_A = \xi_B = 50$ meV at $t = 1$ fs. Since at this time the intensity of the Gaussian shape laser pulse has dropped to about 10% of its peak value, we perform all subsequent time propagations according to the field-free Hamiltonian having the element-specific ξ_A and ξ_B. Using the same excited state for all calculations with different ξ_i allows us to focus on the influence of inhomogeneities in the SOC on the postexcitation spin dynamics of the ferromagnet, by avoiding to introduce

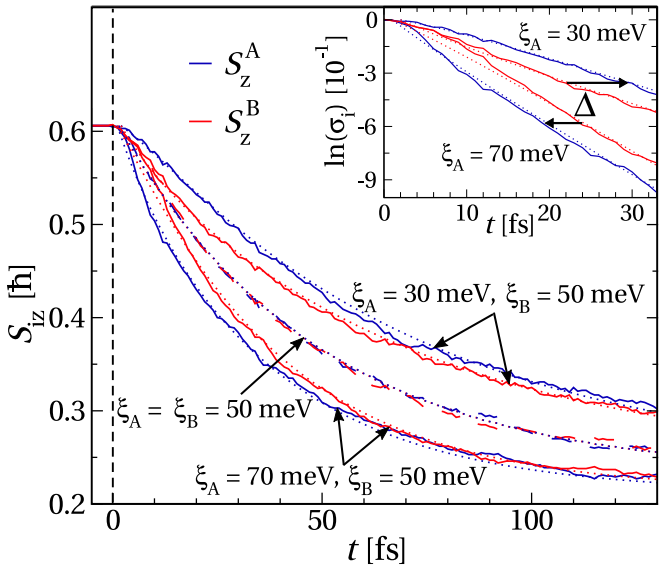

FIG. 4. Average spin magnetization $S_{iz}(t)$ at atoms A (blue curves) and B (red curves) as a function of time t, for $\xi_B = 50$ meV and different spin-orbit coupling strengths ξ_A at sublattice A. In all cases the same initial excited state obtained by laser excitation of the homogeneous system with $\xi_A = \xi_B = 50$ meV (dashed curves) is considered. The dotted curves are obtained by fitting the solution of the phenomenological rate equations (6) and (7) to the corresponding exact time propagations $S_{iz}(t)$. In the inset, the logarithm of the normalized magnetization change $\sigma_i(t) = [S_{iz}(t) - S_{iz}(\infty)]/[S_{iz}^0 - S_{iz}(\infty)]$ is shown as a function of time. The time shifts Δ between the onset of the demagnetization in sublattices A and B are indicated by the horizontal arrows, as obtained from Eq. (8): $\Delta = 8$ fs for $\xi_A = 30$ meV and $\Delta = -5$ fs for $\xi_A = 70$ meV.

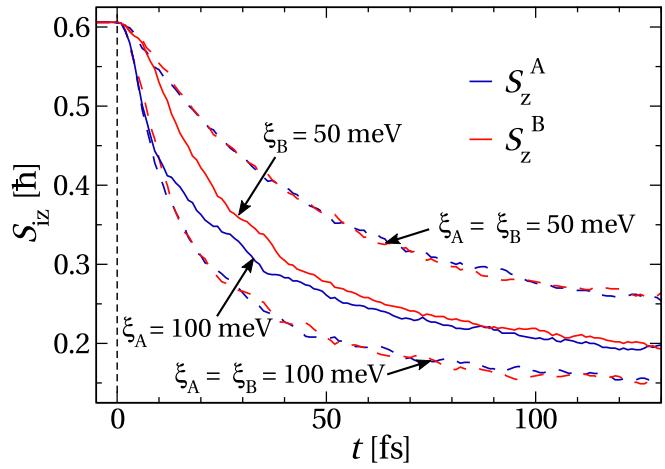

FIG. 5. Average spin magnetization $S_{iz}(t)$ at atoms A (blue curves) and B (red curves) as a function of time t for $\xi_A = 100$ meV and $\xi_B = 50$ meV in comparison with the homogeneous systems having $\xi = 50$ and $\xi = 100$ meV (dashed curves). In all cases the same initial excited state corresponding to the laser excitation of the homogeneous system with $\xi_A = \xi_B = 50$ meV is considered.

any changes in the dynamics resulting from differences in the initial optical absorption.

In Fig. 4 the spin dynamics $S_z^A(t)$ and $S_z^B(t)$ in sublattices A and B are shown for $\xi_A = 30$, 50, and 70 meV. Knowing that the spin-orbit coupling controls the fundamental angular momentum transfer at the origin of the UFD [30] it is not surprising that $S_z^A(t)$ decreases faster (slower) with time when ξ_A is larger (smaller) than in the homogeneous case (dashed curves). An analogous behavior has already been observed by varying ξ in homogeneous systems [30,34]. Element-specific demagnetization times have also been found in experiments on pure TMs [50]. The authors observed that Ni is found to demagnetize more slowly than Fe, which can be interpreted within our model as the consequence of a weaker SOC efficiency of the former. Much more interesting, however, are the significant effects of varying ξ_A on the magnetization dynamics of sublattice B, where the SOC strength has been kept constant. As shown in Fig. 4, smaller (larger) values of ξ_A results in a clearly slower and less strong (faster and stronger) demagnetization at the B atoms. One concludes that the local magnetization dynamics at a given atom i depends not only on the microscopic parameters characterizing this particular atom but also quite remarkably on the properties of its environment.

In order to highlight the role of the local environment, we compare in Fig. 5 the spin dynamics of two homogeneous systems having $\xi = 50$ and $\xi = 100$ meV with the element-specific spin dynamics of the a binary alloy having $\xi_A = 100$ meV and $\xi_B = 50$ meV. One observes that in the alloy the coupling between the sublattices accelerates the demagnetization in sublattice B (faster decrease of S_z^B) while slowing down the demagnetization in sublattice A. In other words, when elements having different SOC efficiencies are mixed, the demagnetization times are increased (reduced) at the elements having a stronger (weaker) SOC. These results are qualitatively in agreement with experiments on FePt, CoPt, and NiPd alloys [54–56,61], which show that replacing Co or Fe by Pt accelerates the demagnetization process. Let us recall that the SOC is much stronger in Pt than in Fe or Co and that the strong hybridization between the Co or Fe and Pt atoms induces significant magnetic moments at the Pt atoms.

In the case of FeNi Mathias *et al.* observed a delay in the onset of the demagnetization at the Ni atoms relative to the Fe ones which is followed by a progressive convergence to a steady demagnetization rate [50]. Similar observations have been made by other groups [48,57–59]. As shown in Figs. 4 and 5, our calculations are in good qualitative agreement with this behavior. In the inset of Fig. 4 the logarithm of the normalized magnetization change $\sigma_i(t) = [S_{iz}(t) - S_{iz}(\infty)]/[S_{iz}^0 - S_{iz}(\infty)]$ for $\xi_A = 30$ and 70 meV is plotted as a function of time. The approximately linear decrease of $\ln(\sigma_i)$ for $t \geqslant 10$ fs reflects the exponential decay of the magnetization once the transient processes immediately following the laser excitation are over. Notice that the slopes of $\ln(\sigma_A)$ and $\ln(\sigma_B)$ are practically the same for $t \geqslant 10$ fs. This corresponds to the steady-state equilibrium that is reached between the various processes involved in the ultrafast demagnetization, namely the local spin-to-orbital angular-momentum transfer at the different alloy components, the orbital-moment quenching and the interatomic spin-density flux. One may then graphically identify the time shift Δ relating the sublattice magnetizations as $\sigma_A(t) \simeq \sigma_B(t - \Delta)$. This corresponds to a delay ($\Delta > 0$) or an advance ($\Delta < 0$) of the demagnetization of sublattice A relative to B depending on whether $\xi_A < \xi_B$ or $\xi_A > \xi_B$

(see the inset of Fig. 4). A quantitative expression for the time shift Δ in the steady state is derived and compared with experimental observations in Secs. IV D and IV E.

C. Phenomenological rate model

The element-specific spin dynamics derived from the many-body time propagations can be analyzed *a posteriori* by considering the coupled rate equations

$$\frac{ds_A}{dt} = -k_A\, s_A + k_{AB}\,(s_B - s_A), \tag{6}$$

and

$$\frac{ds_B}{dt} = -k_B\, s_B - k_{AB}\,(s_B - s_A), \tag{7}$$

where $s_A = S_z^A - S_z^A(\infty)$ and $s_B = S_z^B - S_z^B(\infty)$ denote the time-dependent spin polarizations of sublattices A and B relative to their respective long-time equilibrium values $S_z^A(\infty)$ and $S_z^B(\infty)$. On the one hand, the demagnetization rates k_A and k_B describe the local changes of the spin polarizations of atoms A and B, whose microscopic origin resides in the SOC-induced intra-atomic spin-to-orbital angular-momentum transfer and subsequent orbital-moment quenching. On the other hand, the rate k_{AB} takes into account the spin transfer between the sublattices, where the inverse spin-transfer rate $\tau_{AB} = k_{AB}^{-1}$ gives a measure of the characteristic time involved in the response of the many-body system to inhomogeneities in the spin-density distribution. These equations relate the element-specific spin dynamics of the two sublattices with each other. They allow us to discern the timescales associated to local demagnetization and to interatomic spin transfer.

For the homogeneous system having $\xi_A = \xi_B = 50$ meV (dashed curves in Fig. 4) the best fit of the model to the exact many-body results is obtained with $k_A = k_B = 0.021$ fs^{-1}, independently of the value of k_{AB}. In the case of alloys having different ξ_A and the same $\xi_B = 50$ meV we set $k_B = 0.021$ fs^{-1} for all ξ_A and vary only k_A and k_{AB}. Figure 4 shows that the phenomenological model given by Eqs. (6) and (7) yields very good fits to the exact results, which confirms the validity of picturing the local magnetization dynamics in terms of competing spin-density flows. Moreover, it is interesting to note that the best fits yield almost the same $k_{AB} \simeq 0.05$ fs^{-1} for all ξ_A. This is quite reasonable since k_{AB} reflects the spin-density flux between the two alloy components, which is independent of the local spin-orbit-coupling strengths.

In Fig. 6(a) the optimal local transfer rate k_A is shown as a function of ξ_A where, for simplicity, we have kept $k_{AB} = 0.05$ fs^{-1} constant. The proportionality relation between k_A and ξ_A confirms the interpretation that k_i has its origin in the local spin-orbit interactions at atom i. Figure 6(b) shows the element-specific demagnetization times $\tau_{\rm dm}^i$, which are defined as the time after which $s_i = S_{iz}(t) - S_{iz}(\infty)$ has decreased to a factor $1/e$ of its initial value $\Delta S_{iz} = S_{iz}^0 - S_{iz}(\infty)$. One observes that $\tau_{\rm dm}^A$ decreases with increasing ξ_A approximately as $\hbar/\xi_A$, going from $\tau_{\rm dm}^A = 117$ fs for $\xi_A = 0$ to $\tau_{\rm dm}^A = 12$ fs for $\xi_A = 210$ meV. Thus, the A atoms demagnetize faster (slower) than the B atoms when $\xi_A > \xi_B$ ($\xi_A < \xi_B$). This trend is consistent with previous results on homogeneous systems showing that the SOC strength ξ controls the timescale of the demagnetization process ($\tau_{\rm dm} \propto \hbar/\xi$) [30]. Concerning the B atoms, we observe that $\tau_{\rm dm}^B$ decreases from 93 to 25 fs as ξ_A increases from $\xi_A = 0$ to 210 meV, even though $\xi_B = 50$ meV has been kept constant throughout. One concludes that the rates of change of the local magnetizations are most sensitive to the local environment of the atoms, a further clear indication of the importance of spin-density transfer among the alloy components.

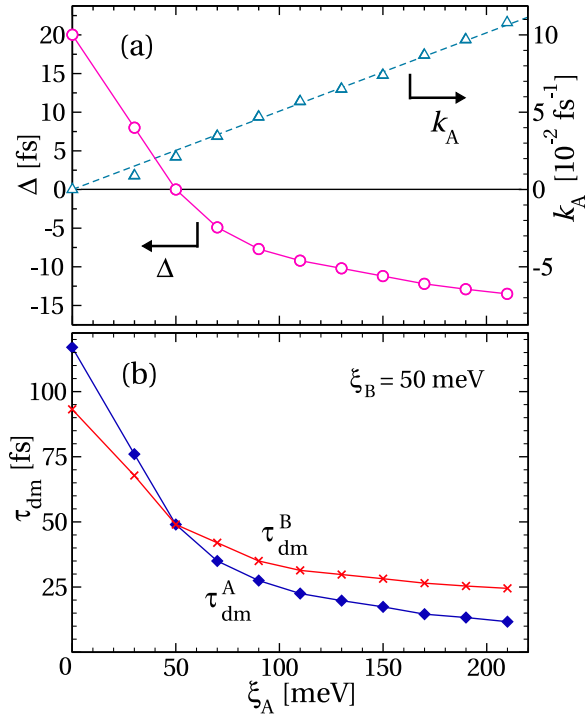

FIG. 6. (a) Local demagnetization rate k_A of sublattice A (blue open triangles) and time shift Δ of the demagnetization of sublattice A with respect to sublattice B (magenta open circles). Results are given as a function of the spin-orbit coupling strength ξ_A at the A atoms for $\xi_B = 50$ meV. k_A is obtained by fitting the solution of the rate equations (6) and (7) to the corresponding exact $S_z^A(t)$ and $S_z^B(t)$ using $k_B = 0.021$ fs^{-1} and $k_{AB} = 0.05$ fs^{-1}. The time shift Δ follows then from Eq. (8). (b) Sublattice demagnetization times $\tau_{\rm dm}^A$ (blue filled rhombus) and $\tau_{\rm dm}^B$ (red crosses). The lines connecting the points and the dashed straight line with $k_A \simeq 5{\times}10^{-4}$ fs^{-1} meV^{-1} ξ_A are a guide to the eyes.

D. Spin-density flow between the sublattices

In order to analyze the spin density flow during the demagnetization dynamics we consider the case $\xi_B = 50$ meV and $\xi_A = 0$, which amounts to neglecting the SOC at the A atoms. This also allows us to simulate physical situations in which the efficacy of spin-orbit transitions at one alloy component is strongly reduced, for example, due to a very large local exchange splitting or a nearly fully occupied d band, in which case any SOC-induced spin-flips take place almost exclusively at the B atoms. The solid curves in Fig. 7 show the exact calculated time dependencies of S_z^A and S_z^B following a 1 fs homogeneous laser-pulse excitation. The spin dynamics of the homogeneous system having $\xi_A = \xi_B = 50$ meV is also displayed for the sake of comparison (dashed curves). One observes that the absence of spin-orbit transitions at the A atoms

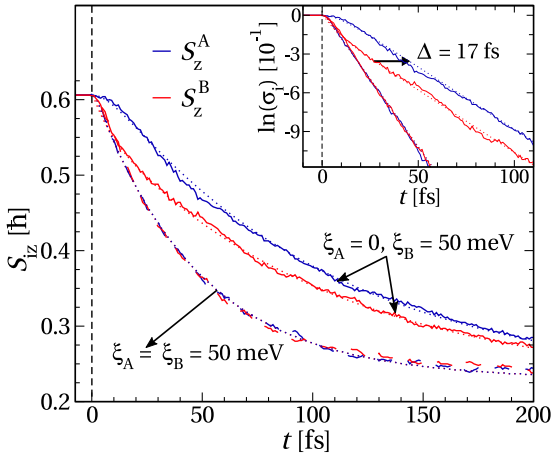

FIG. 7. Time dependence of the local spin magnetization $S_{iz}(t)$ at the A atoms (blue curves) and at the B atoms (red curves) after excitation with a 1 fs laser pulse (homogeneous field). Results are given for a binary alloy having $\xi_A = 0$ and $\xi_B = 50$ meV (solid curves) and for the homogeneous system having $\xi_A = \xi_B = 50$ meV (dashed curves). The dotted curves are obtained by fitting the solution of the phenomenological rate equations (6) and (7) to the exact results. In the inset the logarithm of the normalized magnetization changes $\sigma_i(t)$ are shown. Here the horizontal arrow indicates the delay Δ involved in the onset of the demagnetization of sublattice A, as obtained from Eq. (8).

does not preclude the alloy from demagnetizing throughout and to a comparable extent as in the homogeneous case, albeit more slowly. Indeed, not only the sublattice B but also the sublattice A demagnetizes rapidly as a function of time, within a few hundred femtoseconds. However, notice that the rate of change of S_z^B is significantly smaller than in the homogeneous case, where the SOC is also active in sublattice A. Quantitatively, the demagnetization times obtained from the exponential fits are $\tau_{\rm dm}^A \simeq 117$ fs and $\tau_{\rm dm}^B \simeq 93$ fs for $\xi_A = 0$ and $\xi_B = 50$ meV, while in the homogeneous case we have $\tau_{\rm dm}^A = \tau_{\rm dm}^B \simeq 49$ fs [see Fig. 6(b)]. The fact that sublattice A demagnetizes in an ultrafast way, despite the lack of local spin-to-orbital angular-momentum transfer at the A atoms, confirms the importance of the spin-density flow between the alloy components.

As already observed, the demagnetization timescale $\tau_{\rm dm}^A$ is significantly longer than $\tau_{\rm dm}^B$, which in its turn is longer than the demagnetization time in the homogeneous case. This trend can be qualitatively explained by the fact that the demagnetization of the A atoms necessarily involves a transfer of spin density to the B atoms. One may furthermore notice the presence of a significant time delay $\Delta \simeq 17$ fs in the onset of the demagnetization of sublattice A relative to B, which corresponds to the horizontal shift between $\sigma_A(t)$ and $\sigma_B(t)$ in Fig. 7 [$\sigma_A(t) \simeq \sigma_B(t - \Delta)$]. A similar effect has been observed in experiments on permalloy [48,50,57–59]. Further details are discussed in Sec. IV E.

In order to better understand the origin of the time shift Δ, it is instructive to derive a quantitative expression for it in terms of the demagnetization and spin-transfer rates describing the spin dynamics. Figure 7 shows that after a short transient time of the order of Δ the spin dynamics approaches a steady-state regime where both alloy components demagnetize at the same rate and where $S_z^A(t)$ and $S_z^B(t)$ decay approximately parallel to each other separated by an approximately constant time shift Δ [i.e., $S_z^A(t) \simeq S_z^B(t - \Delta)$]. Using the phenomenological spin-transfer model given by Eqs. (6) and (7) one can in fact show that the solution of these rate equations with equal initial polarizations $s_A(0) = s_B(0)$ approaches such a steady-state regime of the form $s_A(t) = s_B(t - \Delta)$ with the time shift Δ given by

$$\Delta = \frac{1}{k_{AB}} \frac{k_B - k_A}{k_B + k_A}. \tag{8}$$

In this way the experimentally observed time shift can be related to parameters k_A, k_B, and k_{AB} characterizing the spin dynamics in the alloy. In our case we calculate Δ using Eq. (8) once k_A, k_B, and k_{AB} have been fitted to the exact many-body propagations. The quality of these fits can be assessed by comparing full and dotted curves in Figs. 4, 7, and 8. Keeping $\xi_B = 50$ meV fixed, we obtain $\Delta = 17$ fs for $\xi_A = 0$, $\Delta = 8$ fs for $\xi_A = 30$ meV and $\Delta = -5$ fs for $\xi_A = 70$ meV (see the insets of Figs. 4 and 7). The correlation between the increase of k_A and the decrease and change of sign of Δ with increasing ξ_A is also demonstrated in Fig. 6(a), where ξ_A is varied for constant ξ_B.

The results discussed in this section have shown that the spin-density exchange between different components plays a central role in the laser-induced magnetization dynamics of metallic alloys. At the origin of such laser-triggered spin-density flows one finds the electronic hybridizations, which are responsible of metallic binding and which control the timescale of the electronic motion in the lattice. They are therefore expected to play a key role in understanding of the demagnetization in multicomponent systems. In the following section, the dependence of the magnetization dynamics on the interatomic hopping integrals is analyzed in some detail.

E. Role of interlattice hybridizations

A more detailed insight into the spin-density flow across the alloy and into the resulting relation between demagnetization delay and electron delocalization can be achieved by varying the strength of the hybridizations between the sublattices. In the following we consider a binary system with inhomogeneous spin-orbit couplings $\xi_A = 0$ and $\xi_B = 50$ meV. The hopping integrals between the atoms belonging to different sublattices A and B are scaled as $t_{ij} = \alpha\, t_{ij}^0$ with $\alpha \leqslant 1$, while the hopping integrals between atoms of the same kind remain equal to the original t_{ij}^0 derived from band-structure calculations. The obtained element-specific dynamics of S_z^A and S_z^B are shown in Fig. 8, where the solid curves correspond to the exact calculated time evolution and the dotted curves to the best fits obtained by applying the rate equations (6) and (7). First, one observes that the strength of the A − B hybridizations does not significantly affect the ultimate degree of demagnetization $\Delta S_z = S_z^0 - S_z(\infty)$. Indeed, for all considered α, the A atoms reach the same degree of demagnetization as the B atoms, despite the fact that $\xi_A = 0$ [79]. This is the consequence of the spin polarization transfer between the two alloy components discussed in Sec. IV B, which remains valid even when the strength

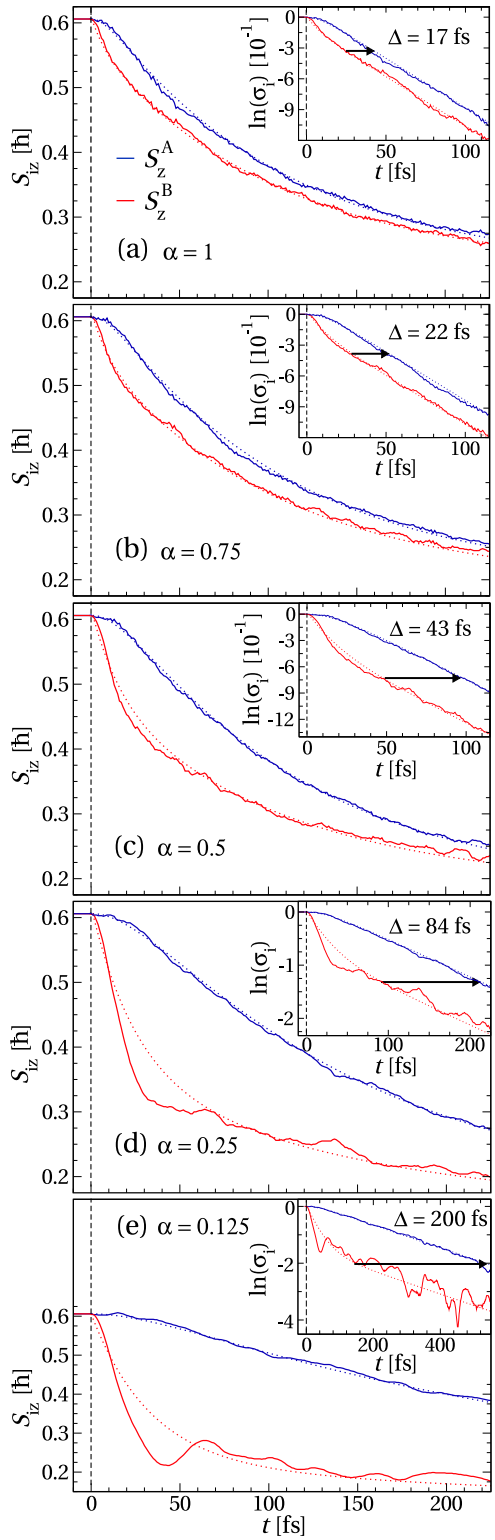

FIG. 8. Time dependence of the local spin moments S_z^A (blue curves) and S_z^B (red curves) in a laser-excited binary alloy having $\xi_A = 0, \xi_B = 50$ meV and representative values of the scaled hopping integrals $t_{ij} = \alpha\, t_{ij}^0$ between the sublattices A and B. The solid curves are the result of exact time propagations, while the dotted curves are obtained by fitting the phenomenological rate equations (6) and (7). The insets show the logarithm of the normalized magnetization change $\sigma_i(t) = [S_{iz}(t) - S_{iz}(\infty)]/[S_{iz}^0 - S_{iz}(\infty)]$. The indicated time delays Δ have been determined using Eq. (8).

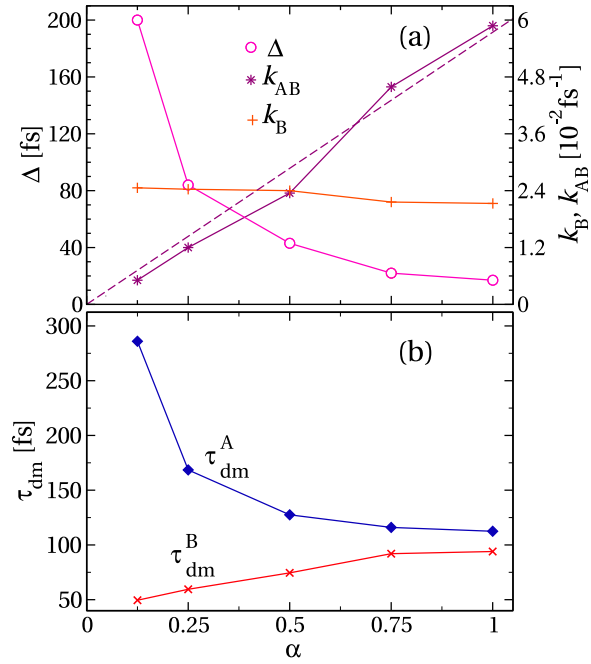

FIG. 9. (a) Time shift Δ (magenta open circles) of the demagnetization of sublattice A with respect to sublattice B, interlattice spin-transfer rate k_{AB} (purple asterisks) and local demagnetization rate k_B (orange plus signs) as functions of the relative strength $\alpha = t_{ij}/t_{ij}^0$ of the hybridizations between the sublattices A and B. The hopping integrals between atoms of the same kind remain in all cases equal to the reference band-structure values t_{ij}^0. The results are derived from the fits to the exact time dependencies of $S_z^A(t)$ and $S_z^B(t)$ using the rate equations (6) and (7), which are shown in Fig. 8 [see also Eq. (8)]. (b) Sublattice demagnetization times $\tau_{\rm dm}^A$ (blue filled rhombus) and $\tau_{\rm dm}^B$ (red crosses). The lines connecting the points and the dashed straight line with $k_{\rm AB} \simeq (16.7\ {\rm fs})^{-1}\,\alpha$ are a guide to the eyes.

of the hybridizations is diminished ($0 < \alpha < 1$). In contrast, the shape of $S_z^A(t)$ as a function of time is obviously quite sensitive to the strength of the coupling between the sublattices. Comparing the time dependence of $S_z^A(t)$ and $S_z^B(t)$ given in the different subfigures of Fig. 8 demonstrates the development of an increasing delay Δ in the onset of the demagnetization of sublattice A ($\xi_A = 0$) relative to sublattice B ($\xi_B = 50$ meV) as the ratio α between A-B and A-A or B-B hoppings is reduced. Starting from the homogeneous case [$\alpha = 1$ in Fig. 8(a)] where the delay is already significant ($\Delta = 17$ fs) one observes that progressively decreasing the A-B hoppings systematically slows down the demagnetization rate at sublattice A while at the same time the demagnetization at the B atoms is speeded up [Figs. 8(b) and 8(c)]. Compare also the inset figures, where the time shift between the nearly linear decrease of $\ln(\sigma_A)$ and $\ln(\sigma_B)$ for not-too-short times is indicated by the arrows [$\sigma_A(t) \simeq \sigma_B(t - \Delta)$ for $t \gtrsim \Delta$].

This behavior can be essentially traced back to the changes in the spin-transfer rate k_{AB} and timescale $\tau_{AB} = 1/k_{AB}$ as a function of α. As shown in Fig. 9(a), k_{AB} is approximately proportional to α, whereas the local demagnetization rates remain essentially unaffected by the changes in the interlattice hoppings: $k_A = 0$ since $\xi_A = 0$ and k_B depends weakly on α.

Quantitatively, k_{AB} decreases by a factor 10 from $k_{AB} = 0.059$ fs^{-1} ($\tau_{AB} = 17$ fs) to $k_{AB} = 0.005$ fs^{-1} ($\tau_{AB} = 200$ fs) as α is reduced from 1 to 0.125. In the same range of α k_B changes to a much lesser extent, from 0.021 to 0.025 fs^{-1} [see Fig. 9(a)]. This is consistent with the fact that the spin-density transfer between sublattices is a direct consequence of the electronic motion between the different atoms. The weak dependence of k_B on α can be explained by recalling that k_A and k_B are mainly controlled by the local spin-orbit coupling strengths ξ_A and ξ_B, respectively, which have been kept constant throughout these calculations (see also Sec. IV C).

In Fig. 9(a) Δ is shown as a function of α. The delay in the demagnetization at the A atoms with respect to the B atoms can be qualitatively explained by recalling that the decrease of S_z^B starts as soon as the laser excites them, since it is driven by the SOC-induced spin-flips taking place directly at the B atoms ($\xi_B \neq 0$). In contrast, a demagnetization in A can only be the result of spin transfers between the two sublattices which tends to reestablish a homogeneous spin-density distribution. Since $k_A = 0$, Eq. (8) implies that $\Delta = \tau_{AB} = 1/k_{AB}$ coincides with the inverse spin-transfer rate between the sublattices. Thus, Δ gives a measure of the response of the many-body system to changes in the spin-density distribution throughout the alloy. Consequently, when the hopping integrals between the A and B atoms are reduced ($\alpha < 1$) the reaction of sublattice A to the incipient demagnetization in sublattice B is slower, causing Δ to increase.

The trends derived from our calcultions should be compared with the UFD experiments on permalloys [41,48,50,57–60]. In Ref. [50] one observes that the laser-induced demagnetization of the Fe and Ni atoms in the $Ni_{80}Fe_{20}$ permalloy takes place at similar rates. However, the demagnetization of Fe preceeds that of Ni by approximately $\Delta \simeq 10$–20 fs. Similar observations have been made by other groups [48,57–59]. Furthermore, when Cu is added to the permalloy and the direct magnetic interactions between the Fe and Ni atoms are in average reduced, one observes that the delay in the onset of the demagnetization at the Ni atoms increases to $\Delta \simeq 76$ fs [50]. Our calculations, where the decrease in FeNi hybridizations is modeled by a reduction of the hoppings between the two sublattices, show qualitatively similar trends (see Figs. 8 and 9). Decreasing the interlattice hoppings from $t_{ij} = t_{ij}^0$ to $t_{ij} = t_{ij}^0/4$ results in an increase of the delay Δ from 17 to 84 fs, which is in good agreement with the measured values. In this context, it is also important to note that other UFD experiments on permalloys [41,60] have not reported a significant delay between Ni and Fe. This could be due to different experimental conditions.

Finally, it is interesting to consider the dependence of the element-specific demagnetization times $\tau_{\rm dm}^i$ on the hybridizations between the sublattices. Figure 9(b) shows that at the B atoms $\tau_{\rm dm}^B$ decreases from 94 to 50 fs as interlattice hoppings $t_{ij} = \alpha t_{ij}^0$ are reduced. Qualitatively, the weaker the majority spin-density flux arriving to sublattice B from A, the faster the rate at which the B atoms can be demagnetized by the local spin-to-orbital angular-momentum transfer due to spin-orbit interactions. In other words, a stronger spin imbalance between S_z^B and S_z^A needs to be established in order to reach the steady-state regime. In contrast, at sublattice A, $\tau_{\rm dm}^A$ increases significantly from 113 to 286 fs with decreasing α. These results are not only consistent with the local origin of the demagnetization process at the B atoms but they also confirm the importance of the spin-density flux across the alloy which is driven by the hybridizations between the different alloy components.

V. CONCLUSION

The optically-triggered magnetization dynamics of transition-metal binary alloys has been investigated in the framework of a many-body electronic theory by performing exact time propagations on a tetrahedral cluster model. The dependence of the magnetic response on the main microscopic parameters characterizing the alloy components has been determined, by paying special attention to understanding how the various element-specific local magnetic behaviors are interrelated as a function of time and how they give rise to the global demagnetization. In the case where the laser absorption is inhomogeneous, we observe remarkably rapid spin transfers among the alloy components at the very early stages of the dynamics, which physically corresponds to the OISTR previously demonstrated in time-dependent density-functional studies [31,68]. A local insight into the OISTR effect is provided, which involves an initial local optical excitation followed by a rapid redistribution of the spin-polarized density driven by the interatomic hoppings. Any laser-induced disparities among the excitation levels and local electronic occupations of the different elements are found to be washed away within a few femtoseconds by the large mobility of the itinerant d electrons.

The magnetization dynamics of the alloys has been shown to be very sensitive to inhomogeneities in the strength and effectiveness of the spin-orbit interactions. Element-specific demagnetization times as well as remarkable delays (respectively, advances) in the onset of the ultrafast demagnetization at different alloy components have been demonstrated. The local magnetization dynamics at atoms having a strong and efficient SOC is slowed down with respect to its pure-element value (as measured, for example, by the demagnetization rate $k_{\rm dm} = \tau_{\rm dm}^{-1}$) when they are alloyed with elements where the SOC is weak or inefficient. Conversely, the demagnetization rate at atoms with weak SOC is accelerated by alloying them with strong spin-orbit coupling elements. This experimentally observed interdependence [54–56,61] has been shown to be a consequence of the spin-density flow associated to the motion of the itinerant d electrons responsible of magnetism.

Furthermore, since the atoms showing a stronger or more efficient SOC demagnetize faster than those having weaker SOC, time delays Δ build up in the demagnetization of the latter before a steady-state regime is reached. It has been shown that the importance of the delay Δ can be enhanced by reducing the spin-density transfer rate between different magnetic components of the alloy. This can be modified, for example, by reducing the interlattice hopping integrals, as in the present calculations, by introducing vacancies or by alloying with nonmagnetic elements. Qualitatively similar trends have been observed in experiments [48,50,57–59].

A simple phenomenological model has been introduced in order to analyze and interpret the exact many-body time propagations. In this way the interplay between local,

spin-orbit mediated demagnetizations and interatomic spin-density exchanges has been revealed. Despite its simplicity a remarkably good agreement with the exact many-body propagations has always been obtained, once the rate constants are appropriately fitted. This not only demonstrates the validity of picturing the alloy dynamics in terms of local demagnetizations and interatomic spin flow, but also allows us to identify and discern these two main physically distinct processes, the former being governed by the SOC and the latter being driven by the interatomic hoppings.

The above conclusions reflect the intrinsic collective dynamics of the itinerant electrons responsible for magnetism. They should be therefore qualitatively valid also when other forms of excitations are used to trigger the initial out-of-equilibrium state (e.g., hot electrons or spin-polarized current pulses). The present study emphasizes the fundamental role played by both the spin-orbit-driven local spin-flip transitions and the spin-conserving electronic motion in the ultrafast magnetization dynamics of TM compounds.

ACKNOWLEDGMENTS

One of the authors (G.S.) gratefully acknowledges the support by the Graduate Academy of the University of Kassel. Computer resources were supplied by the IT Service Center of the University of Kassel and by the Goethe Center for Scientific Computing of the University of Frankfurt.

[1] E. Beaurepaire, J.-C. Merle, A. Daunois, and J.-Y. Bigot, Phys. Rev. Lett. **76**, 4250 (1996).
[2] G. P. Zhang and W. Hübner, Phys. Rev. Lett. **85**, 3025 (2000).
[3] G. Lefkidis and W. Hübner, Phys. Rev. B **76**, 014418 (2007).
[4] M. Krauß, T. Roth, S. Alebrand, D. Steil, M. Cinchetti, M. Aeschlimann, and H. C. Schneider, Phys. Rev. B **80**, 180407(R) (2009).
[5] B. Mueller, M. Haag, and M. Fähnle, J. Magn. Magn. Mater. **414**, 14 (2016).
[6] M. Lisowski, P. A. Loukakos, A. Melnikov, I. Radu, L. Ungureanu, M. Wolf, and U. Bovensiepen, Phys. Rev. Lett. **95**, 137402 (2005).
[7] E. Carpene, E. Mancini, C. Dallera, M. Brenna, E. Puppin, and S. De Silvestri, Phys. Rev. B **78**, 174422 (2008).
[8] A. B. Schmidt, M. Pickel, M. Donath, P. Buczek, A. Ernst, V. P. Zhukov, P. M. Echenique, L. M. Sandratskii, E. V. Chulkov, and M. Weinelt, Phys. Rev. Lett. **105**, 197401 (2010).
[9] M. Haag, C. Illg, and M. Fähnle, Phys. Rev. B **90**, 014417 (2014).
[10] B. Koopmans, H. H. J. E. Kicken, M. van Kampen, and W. J. M. de Jonge, J. Magn. Magn. Mater. **286**, 271 (2005).
[11] B. Koopmans, J. J. M. Ruigrok, F. Dalla Longa, and W. J. M. de Jonge, Phys. Rev. Lett. **95**, 267207 (2005).
[12] M. Cinchetti, M. Sánchez Albaneda, D. Hoffmann, T. Roth, J.-P. Wüstenberg, M. Krauß, O. Andreyev, H. C. Schneider, M. Bauer, and M. Aeschlimann, Phys. Rev. Lett. **97**, 177201 (2006).
[13] D. Steiauf and M. Fähnle, Phys. Rev. B **79**, 140401(R) (2009).
[14] D. Steiauf, C. Illg, and M. Fähnle, J. Magn. Magn. Mater. **322**, L5 (2010).
[15] B. Koopmans, G. Malinowski, F. Dalla Longa, D. Steiauf, M. Fähnle, T. Roth, M. Cinchetti, and M. Aeschlimann, Nat. Mater. **9**, 259 (2010).
[16] A. J. Schellekens and B. Koopmans, Phys. Rev. B **87**, 020407(R) (2013).
[17] C. Illg, M. Haag, and M. Fähnle, Phys. Rev. B **88**, 214404 (2013).
[18] B. Y. Mueller, A. Baral, S. Vollmar, M. Cinchetti, M. Aeschlimann, H. C. Schneider, and B. Rethfeld, Phys. Rev. Lett. **111**, 167204 (2013).
[19] T. Tsatsoulis, C. Illg, M. Haag, B. Y. Mueller, L. Zhang, and M. Fähnle, Phys. Rev. B **93**, 134411 (2016).
[20] M. Fähnle, T. Tsatsoulis, C. Illg, M. Haag, B. Y. Müller, and L. Zhang, J. Supercond. Nov. Magn. **30**, 1381 (2017).
[21] M. Battiato, K. Carva, and P. M. Oppeneer, Phys. Rev. Lett. **105**, 027203 (2010).
[22] A. Melnikov, I. Razdolski, T. O. Wehling, E. T. Papaioannou, V. Roddatis, P. Fumagalli, O. Aktsipetrov, A. I. Lichtenstein, and U. Bovensiepen, Phys. Rev. Lett. **107**, 076601 (2011).
[23] D. Rudolf, C. La-O-Vorakiat, M. Battiato, R. Adam, J. M. Shaw, E. Turgut, P. Maldonado, S. Mathias, P. Grychtol, H. T. Nembach, T. J. Silva, M. Aeschlimann, H. C. Kapteyn, M. M. Murnane, C. M. Schneider, and P. M. Oppeneer, Nat. Commun. **3**, 1037 (2012).
[24] M. Battiato, K. Carva, and P. M. Oppeneer, Phys. Rev. B **86**, 024404 (2012).
[25] A. J. Schellekens, W. Verhoeven, T. N. Vader, and B. Koopmans, Appl. Phys. Lett. **102**, 252408 (2013).
[26] J. H. Mentink, J. Hellsvik, D. V. Afanasiev, B. A. Ivanov, A. Kirilyuk, A. V. Kimel, O. Eriksson, M. I. Katsnelson, and T. Rasing, Phys. Rev. Lett. **108**, 057202 (2012).
[27] S. Wienholdt, D. Hinzke, K. Carva, P. M. Oppeneer, and U. Nowak, Phys. Rev. B **88**, 020406(R) (2013).
[28] V. G. Bar'yakhtar, V. Butrim, and B. Ivanov, Jetp Lett. **98**, 289 (2013).
[29] K. Krieger, J. K. Dewhurst, P. Elliott, S. Sharma, and E. K. U. Gross, J. Chem. Theory Comput. **11**, 4870 (2015).
[30] W. Töws and G. M. Pastor, Phys. Rev. Lett. **115**, 217204 (2015).
[31] P. Elliott, T. Müller, J. K. Dewhurst, S. Sharma, and E. K. U. Gross, Sci. Rep. **6**, 38911 (2016).
[32] M. Stamenova, J. Simoni, and S. Sanvito, Phys. Rev. B **94**, 014423 (2016).
[33] K. Krieger, P. Elliott, T. Müller, N. Singh, J. K. Dewhurst, E. K. U. Gross, and S. Sharma, J. Phys.: Condens. Matter **29**, 224001 (2017).
[34] W. Töws and G. M. Pastor, Phys. Rev. B **100**, 024402 (2019).
[35] P. Elliott, N. Singh, K. Krieger, E. Gross, S. Sharma, and J. Dewhurst, J. Magn. Magn. Mater. **502**, 166473 (2020).
[36] J. K. Dewhurst, S. Shallcross, P. Elliott, S. Eisebitt, C. v. Korff Schmising, and S. Sharma, Phys. Rev. B **104**, 054438 (2021).

[37] M. F. Elhanoty, O. Eriksson, R. Knut, O. Karis, and O. Grånäs, Phys. Rev. B **105**, L100401 (2022).
[38] I. Radu, G. Woltersdorf, M. Kiessling, A. Melnikov, U. Bovensiepen, J.-U. Thiele, and C. H. Back, Phys. Rev. Lett. **102**, 117201 (2009).
[39] I. Radu, K. Vahaplar, C. Stamm, T. Kachel, N. Pontius, H. A. Dürr, T. A. Ostler, J. Barker, R. F. L. Evans, R. W. Chantrell, A. Tsukamoto, A. Itoh, A. Kirilyuk, T. Rasing, and A. V. Kimel, Nature (London) **472**, 205 (2011).
[40] T. Ostler, J. Barker, R. Evans, R. Chantrell, U. Atxitia, O. Chubykalo-Fesenko, S. El Moussaoui, L. Le Guyader, E. Mengotti, L. Heyderman, F. Nolting, A. Tsukamoto, A. Itoh, D. Afanasiev, B. Ivanov, A. Kalashnikova, K. Vahaplar, J. Mentink, A. Kirilyuk, T. Rasing, and A. V. Kimel, Nat. Commun. **3**, 666 (2012).
[41] I. Radu, C. Stamm, A. Eschenlohr, F. Radu, R. Abrudan, K. Vahaplar, T. Kachel, N. Pontius, R. Mitzner, K. Holldack, A. Föhlisch, T. A. Ostler, J. H. Mentink, R. Evans, R. W. Chantrell, A. Tsukamoto, A. Itoh, A. Kirilyuk, A. V. Kimel, and T. Rasing, SPIN **05**, 1550004 (2015).
[42] N. Bergeard, V. López-Flores, V. Halté, M. Hehn, C. Stamm, N. Pontius, E. Beaurepaire, and C. Boeglin, Nat. Commun. **5**, 3466 (2014).
[43] M. Hennecke, I. Radu, R. Abrudan, T. Kachel, K. Holldack, R. Mitzner, A. Tsukamoto, and S. Eisebitt, Phys. Rev. Lett. **122**, 157202 (2019).
[44] F. Siegrist, J. A. Gessner, M. Ossiander, C. Denker, Y.-P. Chang, M. C. Schröder, A. Guggenmos, Y. Cui, J. Walowski, U. Martens, J. K. Dewhurst, U. Kleineberg, M. Münzenberg, S. Sharma, and M. Schultze, Nature (London) **571**, 240 (2019).
[45] F. Willems, C. von Korff Schmising, C. Strüber, D. Schick, D. Engel, J. K. Dewhurst, P. Elliott, S. Sharma, and S. Eisebitt, Nat. Commun. **11**, 871 (2020).
[46] E. Golias, I. Kumberg, I. Gelen, S. Thakur, J. Gördes, R. Hosseinifar, Q. Guillet, J. K. Dewhurst, S. Sharma, C. Schüßler-Langeheine, N. Pontius, and W. Kuch, Phys. Rev. Lett. **126**, 107202 (2021).
[47] R. Abrudan, M. Hennecke, F. Radu, T. Kachel, K. Holldack, R. Mitzner, A. Donges, S. Khmelevskyi, A. Deák, L. Szunyogh, U. Nowak, S. Eisebitt, and I. Radu, Phys. Status Solidi RRL **15**, 2100047 (2021).
[48] S. Jana, R. Knut, S. Muralidhar, R. S. Malik, R. Stefanuik, J. Åkerman, O. Karis, C. Schüßler-Langeheine, and N. Pontius, Appl. Phys. Lett. **120**, 102404 (2022).
[49] C. La-O-Vorakiat, M. Siemens, M. M. Murnane, H. C. Kapteyn, S. Mathias, M. Aeschlimann, P. Grychtol, R. Adam, C. M. Schneider, J. M. Shaw, H. Nembach, and T. J. Silva, Phys. Rev. Lett. **103**, 257402 (2009).
[50] S. Mathias, C. La-O-Vorakiat, P. Grychtol, P. Granitzka, E. Turgut, J. M. Shaw, R. Adam, H. T. Nembach, M. E. Siemens, S. Eich, C. M. Schneider, T. J. Silva, M. Aeschlimann, M. M. Murnane, and H. C. Kapteyn, Proc. Natl. Acad. Sci. USA **109**, 4792 (2012).
[51] C. E. Graves, A. H. Reid, T. Wang, B. Wu, S. de Jong, K. Vahaplar, I. Radu, D. P. Bernstein, M. Messerschmidt, L. Müller, R. Coffee, M. Bionta, S. W. Epp, R. Hartmann, N. Kimmel, G. Hauser, H. A., P. Holl, H. Gorke, J. H. Mentink *et al.*, Nat. Mater. **12**, 293 (2013).
[52] E. Turgut, C. La-o-Vorakiat, J. M. Shaw, P. Grychtol, H. T. Nembach, D. Rudolf, R. Adam, M. Aeschlimann, C. M. Schneider, T. J. Silva, M. M. Murnane, H. C. Kapteyn, and S. Mathias, Phys. Rev. Lett. **110**, 197201 (2013).
[53] A. J. Schellekens, N. de Vries, J. Lucassen, and B. Koopmans, Phys. Rev. B **90**, 104429 (2014).
[54] K. C. Kuiper, T. Roth, A. J. Schellekens, O. Schmitt, B. Koopmans, M. Cinchetti, and M. Aeschlimann, Appl. Phys. Lett. **105**, 202402 (2014).
[55] K. Yamamoto, Y. Kubota, M. Suzuki, Y. Hirata, K. Carva, M. Berritta, K. Takubo, Y. Uemura, R. Fukaya, K. Tanaka, W. Nishimura, T. Ohkochi, T. Katayama, T. Togashi, K. Tamasaku, M. Yabashi, Y. Tanaka, T. Seki, K. Takanashi, P. M. Oppeneer, and H. Wadati, New J. Phys. **21**, 123010 (2019).
[56] I. Vaskivskyi, R. S. Malik, L. Salemi, D. Turenne, R. Knut, J. Brock, R. Stefanuik, J. Söderström, K. Carva, E. E. Fullerton, P. M. Oppeneer, O. Karis, and H. A. Dürr, J. Phys. Chem. C **125**, 11714 (2021).
[57] S. Günther, C. Spezzani, R. Ciprian, C. Grazioli, B. Ressel, M. Coreno, L. Poletto, P. Miotti, M. Sacchi, G. Panaccione, V. Uhlíř, E. E. Fullerton, G. De Ninno, and C. H. Back, Phys. Rev. B **90**, 180407(R) (2014).
[58] S. Jana, J. A. Terschlüsen, R. Stefanuik, S. Plogmaker, S. Troisi, R. S. Malik, M. Svanqvist, R. Knut, J. Söderström, and O. Karis, Rev. Sci. Instrum. **88**, 033113 (2017).
[59] C. Möller, H. Probst, J. Otto, K. Stroh, C. Mahn, S. Steil, V. Moshnyaga, G. S. M. Jansen, D. Steil, and S. Mathias, Rev. Sci. Instrum. **92**, 065107 (2021).
[60] X. Liu, A. Merhe, E. Jal, R. Delaunay, R. Jarrier, V. Chardonnet, M. Hennes, S. G. Chiuzbaian, K. Légaré, M. Hennecke, I. Radu, C. v. Korff Schmising, S. Grunewald, M. Kuhlmann, J. Lüning, and B. Vodungbo, Opt. Express **29**, 32388 (2021).
[61] S.-G. Gang, R. Adam, M. Plötzing, M. von Witzleben, C. Weier, U. Parlak, D. E. Bürgler, C. M. Schneider, J. Rusz, P. Maldonado, and P. M. Oppeneer, Phys. Rev. B **97**, 064412 (2018).
[62] M. Hofherr, S. Häuser, J. K. Dewhurst, P. Tengdin, S. Sakshath, H. T. Nembach, S. T. Weber, J. M. Shaw, T. J. Silva, H. C. Kapteyn, M. Cinchetti, B. Rethfeld, M. M. Murnane, D. Steil, B. Stadtmüller, S. Sharma, M. Aeschlimann, and S. Mathias, Sci. Adv. **6**, eaay8717 (2020).
[63] Q. Remy, J. Igarashi, S. Iihama, G. Malinowski, M. Hehn, J. Gorchon, J. Hohlfeld, S. Fukami, H. Ohno, and S. Mangin, Adv. Sci. **7**, 2001996 (2020).
[64] C. D. Stanciu, F. Hansteen, A. V. Kimel, A. Kirilyuk, A. Tsukamoto, A. Itoh, and T. Rasing, Phys. Rev. Lett. **99**, 047601 (2007).
[65] S. Mangin, M. Gottwald, C.-H. Lambert, D. Steil, V. Uhlíř, L. Pang, M. Hehn, S. Alebrand, M. Cinchetti, G. Malinowski, Y. Fainman, M. Aeschlimann, and E. E. Fullerton, Nat. Mater. **13**, 286 (2014).
[66] C. S. Davies, G. Bonfiglio, K. Rode, J. Besbas, C. Banerjee, P. Stamenov, J. M. D. Coey, A. V. Kimel, and A. Kirilyuk, Phys. Rev. Res. **2**, 032044(R) (2020).
[67] G. Malinowski, F. Dalla Longa, J. Rietjens, P. Paluskar, R. Huijink, H. Swagten, and B. Koopmans, Nature (London) **4**, 855 (2008).
[68] J. K. Dewhurst, P. Elliott, S. Shallcross, E. K. U. Gross, and S. Sharma, Nano Lett. **18**, 1842 (2018).
[69] J. Chen, U. Bovensiepen, A. Eschenlohr, T. Müller, P. Elliott, E. K. U. Gross, J. K. Dewhurst, and S. Sharma, Phys. Rev. Lett. **122**, 067202 (2019).

[70] J. K. Dewhurst, S. Shallcross, I. Radu, P. Elliott, C. v. Korff Schmising, and S. Sharma, Appl. Phys. Lett. **120**, 042401 (2022).

[71] D. A. Papaconstantopoulos, *Handbook of the Band Structure of Elemental Solids* (Plenum Press, New York, 1986).

[72] P. Bruno, Physical Origins and theoretical models of magnetic anisotropy, in *Magnetismus von Festkörpern und Grenzflächen* (Forschungszentrum Jülich, Jülich, 1993), Chap. 24.

[73] D. J. Tannor, *Introduction to Quantum Mechanics: A Time-dependent Perspective* (University Science Books, Sausalito, CA, 2007).

[74] The physics of the UFD effect, and in particular the mechanism of angular momentum transfer and the demagnetization timescale τ_{dm}, have been shown to be largely independent of the details of the initial excitation. Nevertheless, some quantitative aspects, such as the degree of demagnetization, do depend sensitively on the total absorbed energy or number of photons. See Ref. [34].

[75] C. Stamm, T. Kachel, N. Pontius, R. Mitzner, T. Quast, K. Holldack, S. Khan, C. Lupulescu, E. F. Aziz, M. Wietstruk, H. A. Dürr, and W. Eberhardt, Nat. Mater. **6**, 740 (2007).

[76] C. Stamm, N. Pontius, T. Kachel, M. Wietstruk, and H. A. Dürr, Phys. Rev. B **81**, 104425 (2010).

[77] C. Boeglin, E. Beaurepaire, V. Halté, V. López-Flores, C. Stamm, N. Pontius, H. A. Dürr, and J.-Y. Bigot, Nature (London) **465**, 458 (2010).

[78] In magnetic TMs like Fe, Co, and Ni the SOC constants ξ are very similar [72]. Nevertheless, the efficiencies of local spin-orbit transitions can differ strongly, since they depend on the details of the DOS and occupation numbers after excitation. For simplicity, these differences in SOC efficiency are modeled in this work by varying ξ_A and ξ_B.

[79] In the case of very small hybridizations between the sublattices, longer times are needed in order to observe that $|S_z^A - S_z^B| \lesssim 0.01\,\hbar$. For example, for $\alpha = 0.25$ convergence is reached at times t of the order of 700 fs after the laser excitation.